Available Online

JOURNAL OF SCIENTIFIC RESEARCH

J. Sci. Res. **14** (2), 483-500 (2022)

www.banglajol.info/index.php/JSR

Modeling of the Peristaltic Lithogeic Bile Flow in the Calculus Duct Under the Influence of Heat Transfer with Slip Boundary Conditions

T. K. Rawat *, S. Kumari, S. P. Singh

Department of Mathematics, Dayalbagh Educational Institute, (Deemed University), Dayalbagh, Agra, U.P. 282005, India

Received 23 September 2021, accepted in final revised form 7 March 2022

Abstract

This paper deals with a mathematical model that represents non-Newtonian bile flow through a calculus duct under the influence of heat transfer with wall slip conditions. The peristaltic flow of bile is characterized by a generalized Carreau's model. An ordinate transformation is initiated to map the cosine geometry of the stone into a rectangular grid. It allows evaluation velocity, pressure distribution, flow rate, and reflux occurrence conditions, adopting the perturbation technique, the analytical solution obtained under various parameters, such as Knudsen number, amplitude ratio, Grashof number, Weissenberg number, and power index. These mathematical expressions are analyzed by plotting the graph in MATLAB R2018b software and observed that the axial velocity and the pressure gradient are strongly affected by heat and wall slip parameters.

Keywords: Peristaltic flow; Heat transfer; Perturbation technique; Calculus duct; Knudsen number; Wall slip conditions; Fluid behavior index.

doi: http://dx.doi.org/10.3329/jsr.v14i2.55882 J. Sci. Res. **14** (2), 483-500 (2022)

1. Introduction

The most common disease of the biliary system is cholelithiasis, which is associated with the formation of stones in the gallbladder and bile ducts. The formation of stone in the biliary system is complicated due to physiological, biochemical, and biomechanical factors such as an unsystematic diet, metabolism, gallbladder dysfunction, etc. Suppose the diameter of the stenosis is less than the diameter of the cystic duct, then calculus moves from the gallbladder to the common bile duct. The presence of stones in the biliary system is a very complicated situation; there is a blockage of the duct by a stone in the major duodenal papilla zone. As a result, the normal bile flow from the liver to the duodenum raises the jaundice risk. Also, the bile components like cholesterol, bile acids, etc., are harmful to humans are accumulated in the human body. Edemskiy *et al.* [1] analyzed Vater's papilla's acute and chronic inflammatory changes. Agarwal *et al.* [2] studied the effects of flow parameters in the diseased cystic duct and analyzed the blockage effect on bile flow.

* *Corresponding author*: tasatanuj@gmail.com

Transportation of physiological fluids induced by a progressive wave of area contraction or expansion along the length of a distensible tube, mixing and transporting the fluid in the direction of propagation is known as peristalsis. The peristaltic flow of many physiological fluids are flow of urine from the kidney to the bladder through the ureter, movement of food through the food tract, the flow of ovum in the female fallopian tube, transport of spermatozoa and swallowing food through the esophagus, flow of bile from gallbladder to pancreatic duct. Many researchers studied the peristaltic motion of fluid for different geometries by using various assumptions such as low Reynolds number, long-wavelength, small amplitude ratio, small Darcy number, creeping flow, etc. Mishra *et al*. [3] developed a mathematical model for peristaltic flow of bile within the porous pathological duct, and the effect of various flow parameters is investigated in detail. Computed results are compared with previously existing analytical results. Kuchumov *et al*. [4] investigated the peristaltic flow of bile through a papilla ampoule with stone and papillary stenosis by considering two cases when the flow rate becomes less than zero pressure were computed and explained pressure rise magnitude corresponding to reflux occurring conditions. Srinivas *et al*. [5] studied the peristaltic flow of Jeffrey fluid through the inclined asymmetric channel and analyzed the effect of slip condition on flow characteristics and pressure drop. Khan *et al.* [6] investigated the peristaltic transport of non-Newtonian fluid in a porous medium in an inclined channel under the influence of variable viscosity and slip conditions. Kuchumov [7] formed a mathematical model of peristaltic lithogenic bile flow through the tapered duct with papillary stenosis and revealed that the amplitude ratio has more effect on the pressure distribution than the Weissenberg number. Maheshbabu *et al*. [8] studied the hall effects on Carreau's fluid in an asymmetric channel and found the pumping of carreau fluid than that of Newtonian fluid and observed that pressure gradient increases with increasing Hartman number. Mahmood *et al*. [9] developed a mathematical model to see lubrication effects on the peristaltic transport of couple stress fluid in an asymmetric channel. It is found that pressure rise increases on increasing lubrication effects. Goud *et al*. [10] discussed the peristaltic movement of Ellis fluid in a vertical uniform channel with wall properties and slip conditions. Pandey *et al.* [11] investigate the transport of a viscoelastic fluid by peristaltic motion in a circular cylinder tube by considering the Jeffery fluid model, low Reynolds number, large wavelength approximation, and the wave equation assumed to propagates along the wall. They also observed that the pressure decreases as the ratio of relaxation time increases, and the average flow rate is less than the maximum flow rate. Tripathi *et al*. [12] developed a biofluid dynamics mathematical model to study the peristaltic viscoelastic biofluid flow through the asymmetric porous channel by considering low Reynolds number and large wavelength ratio approximation. This mathematical model is related to flow in the diseased intestine. Kumari *et al*. [13] analyzed the effect of nonlinear variable viscosity of the bile with slip boundary condition by considering the peristaltic transport of bile in an inclined channel under low Reynolds number and long-wavelength approximation and concluded that velocity and pressure is more in case of linear variation of viscosity as compare to nonlinear variation of viscosity.

Bile is a greenish-yellow bio-fluid produced by hepatocyte cells of the liver; it contains many biochemical substances like cholesterol, bile acids, bile salts, phospholipids pigments (bilirubin and biliverdin), a small amount of copper electrolytic chemical, and other excreted metals. In adults, about one-liter bile is produced in a day. The biliary system consists of the liver, gallbladder, and biliary ducts (left and right hepatic duct, common hepatic duct, cystic duct, common bile duct, and pancreatic duct). These biliary ducts refer to the path by which bile is secreted by the liver and then transported to the duodenum. After passing through several bile ducts, bile is stored and concentrated in the gallbladder; when any food intake, bile is secreted through a cystic duct from the gallbladder to the duodenum through the common bile duct. Bile accelerates the fat absorption process and plays an important role in the absorption of the vitamins like A, D, E, and K. Ooi *et al*. [14] numerically studied the flow of bile in two- and three-dimensional cystic duct models. In the cystic duct model, data was recorded from different patients, and the pressure drops in these models were compared with an idealized straight duct with regular baffles. Kuchumov *et al.* [15] developed an analytical model of the pathological bile flow in the major duodenal papilla duct with calculus. They showed that pathological bile is a thixotropic non-Newtonian fluid. Kuchumov *et al.* [16] experimentally studied the non-Newtonian flow of pathological bile in the biliary system and analyzed the flow characteristic during the gallbladder refilling and emptying condition. This paper deals with mathematical modeling of lithogenic bile flow through calculus duct to obtain hole dynamics flow characteristics of bile under the influence of heat transfer with wall slip condition, which may be helpful in surgery of calculus duct.

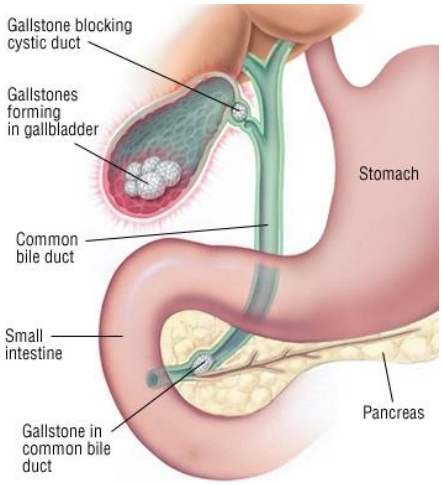

Fig. 1. Biliary system with gallstone [2].

Nomenclature

$(\bar{X}, \bar{Y})$	cartesian coordinates
$(\bar{U}, \bar{V})$	velocity components along $\bar{X}$and $\bar{Y}$ direction
c	wave speed
$\bar{p}$	fluid pressure
g	acceleration due to gravity
C_p	specific heat at constant pressure
Q_0	constant heat addition/absorption
Re	Reynolds number
P_r	Prandtl number
G_r	Grashof number
K	Knudsen number
T_1	temperature at the upper wall
T_0	temperature at the lower wall

Greek symbols

λ	wave length
γ	thermal slip parameter
ρ	density of bile
θ	non dimensional temperature
δ	wave number
β	heat source/sink parameter

Consider the peristaltic flow of an incompressible and non-Newtonian (Carreau's fluid) bile through a calculus (stone) duct with sinusoidal waves of constant speed which propagates along the duct boundaries. The wavenumber δ is infinitely small, and the Reynolds number Re is negligible.

The constitutive relation for the non-Newtonian fluid flow is described in Carreau's equation [7].

$$\overline{S_{ij}} = -p\delta_{ij} + \overline{\tau_{ij}} \tag{1}$$

$$\overline{\tau_{ij}} = \left[\eta_\infty + (\eta_0 - \eta_\infty)(1 + ((\Gamma\bar{\dot{\gamma}})^2)^{\frac{m-1}{2}})\right]\bar{\dot{\gamma}}_{ij} \tag{2}$$

Where p is the pressure, δ_{ij} is Kronecker delta, τ_{ij} is the extra stress tensor, η_0 and η_∞ are the zero and infinite shear rate viscosity, respectively, Γ is the time constant, m is the power index.

The shear rate $\bar{\dot{\gamma}}$ is defined as follows:

$$\bar{\dot{\gamma}} = \sqrt{\frac{1}{2}\sum\sum\bar{\dot{\gamma}}_{ij}\bar{\dot{\gamma}}_{ji}} = \sqrt{\frac{1}{2}\pi} \tag{3}$$

Where π is the second invariant strain rate tensor. In case of η_∞ on applying Taylor's expansion, equation (2) takes the form:

$$\bar{\tau}_{ij} = \eta_0\left[1 + \frac{m-1}{2}((\dot{\gamma})^2)\right]\bar{\dot{\gamma}}_{ij} \tag{4}$$

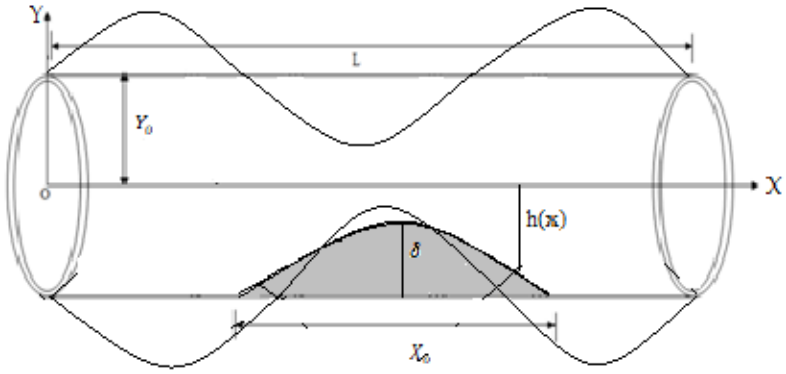

Fig. 2. Geometry of calculus duct.

The effective radius of the duct:

$$\bar{Y}_1(\bar{X},\bar{t}) = \begin{cases} \left[Y_o - \frac{\delta}{2}\left[1 + cos\left\{\frac{\pi(\bar{X}-X_1)}{X_o}\right\}\right].a_1(\bar{t})\right], & d \le X \le d + 2X_o \\ Y_o a_1(\bar{t}), & otherwise, \end{cases} \quad (5)$$

Where $\bar{Y}_1(\bar{X},\bar{t})$ is the radius of the duct segment in the constricted region, $Y_o$the unconstructed radius of the calculus duct, X_o the half-length, δ the maximum width and $X_1$the center of the calculus with δ =0.276Y_o. The time-variant parameter, $a_1(t)$ is given by [17].

$$a_1(\bar{t}) = 1 + K_R \cos(\omega t + \phi)$$

Where K_R represent the amplitude parameter and ϕ the phase angle.
The geometry of the peristaltic wall surface is defined as [17]

$$Y_1(\bar{X},t) = acos\frac{2\pi}{\lambda}\left\{\bar{X} - \frac{k\bar{t}}{X_1}\right\} \quad (6)$$

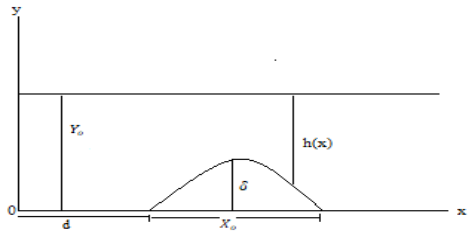

Fig. 3. Schematic diagram of the duct with stone.

The equations of motion are

$$\frac{\partial \bar{U}}{\partial \bar{X}} + \frac{\partial \bar{V}}{\partial \bar{Y}} = 0 \quad (7)$$

$$\rho\left(\frac{\partial}{\partial t}+\bar{U}\frac{\partial}{\partial \bar{X}}+\bar{V}\frac{\partial}{\partial \bar{Y}}\right)\bar{U}=-\frac{\partial \bar{p}}{\partial \bar{X}}+\frac{\partial}{\partial \bar{X}}\bar{\tau}_{\bar{X}\bar{X}}+\frac{\partial}{\partial \bar{Y}}\bar{\tau}_{\bar{X}\bar{Y}}+\rho g\alpha(T-T_0) \quad (8)$$

$$\rho\left(\frac{\partial}{\partial t}+\bar{U}\frac{\partial}{\partial \bar{X}}+\bar{V}\frac{\partial}{\partial \bar{Y}}\right)\bar{V}=-\frac{\partial \bar{p}}{\partial \bar{Y}}+\frac{\partial}{\partial \bar{X}}\bar{\tau}_{\bar{X}\bar{Y}}+\frac{\partial}{\partial \bar{Y}}\bar{\tau}_{\bar{Y}\bar{Y}} \quad (9)$$

$$\rho c_p\left(\frac{\partial \bar{T}}{\partial \bar{t}}+\bar{U}\frac{\partial \bar{T}}{\partial \bar{X}}+\bar{V}\frac{\partial \bar{T}}{\partial \bar{Y}}\right)=K\left(\frac{\partial^2 \bar{T}}{\partial \bar{X}^2}+\frac{\partial^2 \bar{T}}{\partial \bar{Y}^2}\right)+Q_0 \quad 10)$$

Where ρ is the density, $\bar{U}\ and\ \bar{V}$ are the velocity components, $\bar{p}$ is the pressure of the bile. The flow is unsteady in the laboratory frame $(\bar{X},\bar{Y})$. However, in a coordinate system $(\bar{x},\bar{y})$(wave frame) moving with the propagation velocity c, and the boundary shape is stationary.

The transformation from fixed frame to wave frame is given by

$$\bar{x}=\bar{X}-ct\ ,\ \ \bar{y}=\bar{Y},\ \ \bar{u}=\bar{U}-c\ ,\ \ \bar{v}=\bar{V},p=\bar{P},\ \ T=\bar{T} \quad (11)$$

Where $(\bar{u},\bar{v})$ and $(\bar{U},\bar{V})$ are velocity components in the wave and fixed frames, respectively.

Let us introduce the non-dimensional variables.

$$x=\frac{\bar{x}}{\lambda},\quad y=\frac{\bar{y}}{a}\ \ u=\frac{\bar{u}}{c},v=\frac{\bar{v}}{c\delta},\quad p=\frac{a^2}{\lambda c\eta_o}\bar{p},\quad t=\frac{c\bar{t}}{\lambda},\quad \theta=\frac{T-T_0}{T_0},y_1=\frac{\overline{y_1}(\bar{x})}{a},\quad \tau_{xx}=\frac{\lambda}{c\eta_o}\bar{\tau}_{xx},$$

$$\tau_{yy}=\frac{a}{c\eta_o}\bar{\tau}_{yy},\quad \delta=\frac{a}{\lambda},\ We=\frac{c\Gamma}{a},\bar{\dot{\gamma}}=\frac{c\dot{\gamma}}{a}, \quad (12)$$

Using (12), equations (5), (6), (7), (8), (9), and (10) are converted into

$$y_1(x)=\begin{cases}\left[1-\frac{\delta}{2}\left[1+cos\left\{\frac{\pi(x-x_1)}{x_o}\right\}\right]\right], & d\le x\le d+2x_o\\ y_o\ , & otherwise,\end{cases} \quad (13)$$

$$h_1(x)=\phi cos2\pi x \quad (14)$$

$$\delta\frac{\partial u}{\partial x}+\frac{\partial v}{\partial y}=0 \quad (15)$$

$$Re\delta\left(\frac{\partial}{\partial t}+u\frac{\partial}{\partial x}+v\frac{\partial}{\partial y}\right)u=-\frac{\partial p}{\partial x}+\delta\frac{\partial \tau_{xx}}{\partial x}+\frac{\partial \tau_{xy}}{\partial y}+Gr\theta \quad (16)$$

$$Re\delta^3\left(\frac{\partial}{\partial t}+u\frac{\partial}{\partial x}+v\frac{\partial}{\partial y}\right)v=-\frac{\partial p}{\partial y}+\delta^2\frac{\partial \tau_{xy}}{\partial x}+\delta\frac{\partial \tau_{yy}}{\partial y} \quad (17)$$

$$\delta RePr\left(u\frac{\partial \theta}{\partial x}+v\frac{\partial \theta}{\partial y}\right)=\left(\delta^2\frac{\partial^2\theta}{\partial x^2}+\frac{\partial^2\theta}{\partial y^2}\right)+\beta \quad (18)$$

Where $\delta, Re, Gr, P_r, \beta, k_n$ are the non-dimensional parameter, called the wavenumber, Reynolds number, Grashof number, Prandtl number, source/sink parameter, and Knudsen number, respectively, and are defined as

$$Re=\frac{\rho ac}{\eta_o},\ Gr=\frac{\rho g\alpha a^3T_0}{\eta_o c},\ P_r=\frac{\eta_o c_p}{k},\ \beta=\frac{Q_0a^2}{kT_0},\ k_n=\frac{\Lambda}{a} \quad (19)$$

The equation which governs the flow in terms of the stream function $\Psi(x,y)$ after eliminating pressure gradient from equations (16) and (17) we get

$$Re\delta^3\left[\left(\frac{\partial\psi}{\partial y}\frac{\partial}{\partial x}-\frac{\partial\psi}{\partial x}\frac{\partial}{\partial y}\right)\left(\delta\frac{\partial^2\psi}{\partial x^2}+\frac{\partial^2\psi}{\partial y^2}\right)\right]=\left(\frac{\partial^2}{\partial y^2}-\delta^2\frac{\partial^2}{\partial x^2}\right)\tau_{xy}+\delta\left[\frac{\partial^2}{\partial x\partial y}\left(\tau_{xx}-\tau_{yy}\right)\right]+Gr\frac{\partial\theta}{\partial y} \quad (20)$$

Where;

$$\mathrm{u}=\frac{\partial\Psi}{\partial y}, v=-\delta\ \frac{\partial\Psi}{\partial x} \quad (21)$$

Equations (16) and (17) for pressure gradient becomes

$$\frac{\partial p}{\partial x}=\delta\frac{\partial}{\partial x}\tau_{xx}+\frac{\partial}{\partial y}\tau_{xy}-Re\delta\left[\left(\frac{\partial\psi}{\partial y}\frac{\partial}{\partial x}-\frac{\partial\psi}{\partial x}\frac{\partial}{\partial y}\right)\left(\frac{\partial\psi}{\partial y}\right)\right]+Gr\theta \quad (22)$$

$$\frac{\partial p}{\partial y}=\delta^2\frac{\partial}{\partial x}\tau_{xy}+\delta\frac{\partial}{\partial y}\tau_{yy}+Re\delta^3\left[\left(\frac{\partial\psi}{\partial y}\frac{\partial}{\partial x}-\frac{\partial\psi}{\partial x}\frac{\partial}{\partial y}\right)\left(\frac{\partial\psi}{\partial x}\right)\right] \quad (23)$$

2. Volumetric Flow Rate and Boundary Conditions

The dimensionless fluid flow in the fixed frame is

$$Q=\int_0^{\bar{h}(\bar{X},\mathrm{t})}\bar{U}(\bar{X},\bar{Y},\mathrm{t})\mathrm{d}\bar{Y} \quad (24)$$

and equation (24) with wave frame becomes

$$q=\int_0^{\bar{h}(\bar{x})}\bar{u}(\bar{x},\bar{y})\mathrm{d}\bar{y} \quad (25)$$

Using equations (11), (24) and (25) we can write

$$\mathrm{Q}=\mathrm{q}+\frac{\bar{h}^2}{2} \quad (26)$$

The time-mean flow over a period T at a fixed position X is given

$$\bar{Q}=\frac{1}{T}\int_0^T Q\,dt \quad (27)$$

The above expression after using equation (26), becomes

$$\bar{Q}=q+ca \quad (28)$$

dimensionless time-mean flow $\xi\,and\,\Theta$ in the fixed frame and wave frame are

$$\bar{\xi}=\frac{\bar{Q}}{ac},\ \Theta\ =\frac{q}{ac} \quad (29)$$

Using equations (28) and (29), we get

$$\bar{\xi}=\Theta\ +\frac{\bar{h}^2}{2}=\ \Theta\ +\frac{1}{2}\left(h^2(z)+\frac{\phi^2}{2}\right) \quad (30)$$

$$\Theta\ =\int_0^h\frac{\partial\Psi}{\partial y}dy=\ \Psi(h)-\Psi(0) \quad (31)$$

The boundary conditions for the dimensionless stream function in the wave frame are

$$\frac{\partial\theta}{\partial y}=0\quad at\quad y=0 \quad (32)$$

$$\theta=0\quad at\quad y=h(x) \quad (33)$$

$$\Psi=0\quad on\quad y=0\ \text{(by convention)} \quad (34)$$

$$\frac{\partial^2\Psi}{\partial y^2}=0\ \ on\ \ y=0\ \text{(by symmetry)} \quad (35)$$

$$\frac{\partial \Psi}{\partial y} = -1 + K_n \frac{\partial^2 \Psi}{\partial y^2} \ \ on\ y = h(x) \ \text{(wall slip condition)} \tag{36}$$

$$\Psi = \frac{\theta}{2} \ on\ y = h(x) \tag{37}$$

where

$h(x) = y_1(x) + h_1(x)$ (Combined the equation of effective radius of the duct and peristaltic wall surface)

3. An Approximate Solution of the Problem

Considering long-wavelength (δ "1) and low Reynolds number the equations (18), (20), (21), (22), and (23) becomes,

$$\tau_{xy} = \left[1 + \frac{m-1}{2} We^2 \left(\frac{\partial^2 \Psi}{\partial y^2}\right)^2\right]\left(\frac{\partial^2 \Psi}{\partial y^2}\right) \tag{38}$$

$$\frac{\partial^2}{\partial y^2}\left[\left(\frac{\partial^2 \Psi}{\partial y^2}\right) + \frac{m-1}{2} We^2 \left(\frac{\partial^2 \Psi}{\partial y^2}\right)^3\right] + Gr \frac{\partial \theta}{\partial y} = 0 \tag{39}$$

$$\frac{\partial p}{\partial x} = \frac{\partial}{\partial y}\left[\left(\frac{\partial^2 \Psi}{\partial y^2}\right) + \frac{m-1}{2} We^2 \left(\frac{\partial^2 \Psi}{\partial y^2}\right)^3\right] + Gr\theta \tag{40}$$

$$\frac{\partial p}{\partial y} = 0 \tag{41}$$

$$\frac{\partial^2 \theta}{\partial y^2} + \beta = 0 \tag{42}$$

Solving equation (42) using the boundary conditions (32) and (33), we get

$$\theta = \frac{\beta}{2}(h^2 - y^2) \tag{43}$$

The perturbation technique mainly depends on the small parameter of Carreau's fluid (We^2). To solve the nonlinear system of equations (39) and (40) for appropriate boundary conditions as given by equation (34) - (37) as:

$$u = u_0 + We^2 u_1 + O(We^4) \ldots,$$

$$\Psi = \Psi_0 + We^2 \Psi_1 + O(We^4) \ldots, \tag{44}$$

$$p = p_0 + We^2 p_1 + O(We^4) \ldots, \tag{45}$$

$$\Theta = \Theta_0 + We^2 \Theta_1 + O(We^4) \ldots, \tag{46}$$

Where u_0, Ψ_0, p_0 and Θ_0 is the zeroth-order quantities and u_1, Ψ_1, p_1 and Θ_1 is the first-order quantities Substituting equations (39) and (40) in equations for boundary conditions (34) - (37) and collecting the like power of We^2, we obtain zeroth and first-order systems of partial differential equations with corresponding boundary conditions.

3.1. *Zeroth order system*

In zero order system, the absence of Weissenberg number We^2 is taken, the zero-order system without any non-Newtonian parameter is as follows:

$$\frac{\partial^2}{\partial y^2}\left(\frac{\partial^2 \Psi_0}{\partial y^2}\right) + Gr\frac{\partial \theta}{\partial y} = 0 \tag{47}$$

$$\frac{\partial \mathrm{p}_0}{\partial x} = \frac{\partial^3 \Psi_0}{\partial y^3} + Gr\theta \tag{48}$$

$\Psi_0 = 0$ at y = 0 (49)

$$\frac{\partial^2 \Psi_0}{\partial y^2} = 0 \;\; at \;\; y = 0, \tag{50}$$

$$\frac{\partial \Psi_0}{\partial y} = -1 + K_n \frac{\partial^2 \Psi_0}{\partial y^2} \;\; on\; y = h \text{ (wall slip condition)} \tag{51}$$

$$\Psi_0 = \frac{\Theta_0}{2} \; on\; y = h \tag{52}$$

3.2. *The first-order system*

The zero-order solutions obtained from the zero-order system will be combined with the first-order system to obtain a non-homogeneous set of linear partial differential equations.

$$\frac{\partial^2}{\partial y^2}\left[\left(\frac{\partial^2 \Psi_1}{\partial y^2}\right) + \frac{m-1}{2}\left(\frac{\partial^2 \Psi_0}{\partial y^2}\right)^3\right] = 0 \tag{53}$$

$$\frac{\partial p_1}{\partial x} = \frac{\partial}{\partial y}\left[\left(\frac{\partial^2 \Psi_1}{\partial y^2} + \frac{m-1}{2}\left(\frac{\partial^2 \Psi_0}{\partial y^2}\right)^3\right)\right] \tag{54}$$

$\Psi_1 = 0$ at y = 0 (55)

$$\frac{\partial^2 \Psi_1}{\partial y^2} = 0 \;\; at \;\; y = 0, \tag{56}$$

$$\frac{\partial \Psi_1}{\partial y} = -1 + K_n \frac{\partial^2 \Psi_1}{\partial y^2} \;\; on\; y = h \text{ (wall slip condition)} \tag{57}$$

$$\Psi_1 = \frac{\Theta_1}{2} \; on\; y = h \tag{58}$$

On solving the equations (47), (48), and equations (53), (54) and their respective boundary conditions, we obtain the solution of stream function, axial velocity, and pressure gradient of zeroth and first-order system, respectively.

3.2.1. *Zero-order system solution*

$$\Psi_0 = A_1 + A_2 y + A_3 \frac{y^2}{2} + A_4 \frac{y^3}{6} + \frac{Gr\beta y^5}{120}$$

$$u_0 = A_2 + A_3 y + A_4 \frac{y^2}{3} + \frac{Gr\beta y^4}{24}$$

$$\frac{\partial \mathrm{p}_0}{\partial x} = A_4$$

3.2.2. *First-order system solution*

$$\Psi_1 = B_1 + B_2 y + B_3 \frac{y^2}{2} + B_4 \frac{y^3}{6} - \left(\frac{m-1}{2}\right)\left(\frac{{A_4}^3 y^5}{20} + \frac{Gr^3\beta^3 y^{11}}{23760} + \frac{{A_4}^2 Gr\beta y^7}{84} + \frac{A_4 Gr^2\beta^2 y^9}{864}\right)$$

$$u_1 = B_2 + B_3 y + B_4 \frac{y^2}{2} - \left(\frac{m-1}{2}\right)\left(\frac{{A_4}^3 y^4}{4} + \frac{Gr^3\beta^3 y^{10}}{1080} + \frac{{A_4}^2 Gr\beta y^6}{12} + \frac{A_4 Gr^2\beta^2 y^8}{96}\right)$$

$$\frac{\partial p_1}{\partial x} = \left(\frac{3}{3h^2-h^3}\right)\left(\left(\frac{m-1}{2}\right)\left(\frac{{A_4}^3 h^5}{5} - {A_4}^3 h^4 + \frac{Gr^3\beta^3 h^{11}}{2376} - \frac{Gr^3\beta^3 h^{10}}{216} + \frac{{A_4}^2 Gr\beta h^7}{14} - \frac{{A_4}^2 Gr\beta h^6}{2} + \frac{A_4 Gr^2\beta^2 h^9}{108} - \frac{A_4 Gr^2\beta^2 h^8}{12}\right) - \left(\frac{\boldsymbol{Q_1}+2h}{2}\right)\right)$$

3.2.3. *The solution satisfying the corresponding boundary condition*

$$\Psi = A_1 + A_2 y + A_3 \frac{y^2}{2} + A_4 \frac{y^3}{6} + \frac{Gr\beta y^5}{120} + We^2\left(B_1 + B_2 y + B_3 \frac{y^2}{2} + B_4 \frac{y^3}{6} - \left(\frac{m-1}{2}\right)\left(\frac{{A_4}^3 y^5}{20} + \frac{Gr^3\beta^3 y^{11}}{23760} + \frac{{A_4}^2 Gr\beta y^7}{84} + \frac{A_4 Gr^2\beta^2 y^9}{864}\right)\right)$$

$$u = A_2 + A_3 y + A_4 \frac{y^2}{3} + \frac{Gr\beta y^4}{24} + We^2\left(B_2 + B_3 y + B_4 \frac{y^2}{2} - \left(\frac{m-1}{2}\right)\left(\frac{{A_4}^3 y^4}{4} + \frac{Gr^3\beta^3 y^{10}}{1080} + \frac{{A_4}^2 Gr\beta y^6}{12} + \frac{A_4 Gr^2\beta^2 y^8}{96}\right)\right)$$

$$\frac{\partial p}{\partial x} = \left(\frac{1}{3h^2K_n - h^3}\right)\left(\frac{15q_0 + 30h - 5h^4 K_n Gr\beta + h^5 Gr\beta}{10}\right) + We^2\left(\frac{3}{3h^2-h^3}\right)\left(\left(\frac{m-1}{2}\right)\left(\frac{{A_4}^3 h^5}{5} - {A_4}^3 h^4 + \frac{Gr^3\beta^3 h^{11}}{2376} - \frac{Gr^3\beta^3 h^{10}}{216} + \frac{{A_4}^2 Gr\beta h^7}{14} - \frac{{A_4}^2 Gr\beta h^6}{2} + \frac{A_4 Gr^2\beta^2 h^9}{108} - \frac{A_4 Gr^2\beta^2 h^8}{12}\right) - \left(\frac{\boldsymbol{Q_1}+2h}{2}\right)\right)$$

The non-dimensional expression for the pressure rise at the wall in the length of duct L is given by

$$\Delta p = \int_0^L \frac{\partial p}{\partial x} dx = \int_0^d \frac{\partial p}{\partial x} dx + \int_d^{d+x_0} \frac{\partial p}{\partial x} dx + \int_{d+x_0}^L \frac{\partial p}{\partial x} dx$$

WhereA_1, A_2, A_3, A_4, B_1, B_2, B_3 and B_4 are constants, and its values are as follows

$$A_1 = A_3 = B_1 = B_3 = 0$$

$$A_2 = \left(\frac{60\boldsymbol{Q_0} - h^4 Gr\beta - 20A_4 h^2}{120h}\right)$$

$$A_4 = \left(\frac{1}{3h^2K_n - h^3}\right)\left(\frac{15\boldsymbol{Q_0} + 30h - 5h^4 K_n Gr\beta + h^5 Gr\beta}{10}\right)$$

$$B_2 = \left(\frac{3\boldsymbol{Q_1} - B_4 h^3}{6h}\right) - \left(\frac{m-1}{2}\right)\left(\frac{{A_4}^3 h^4}{4} + \frac{Gr^3\beta^3 h^{10}}{2376} + \frac{{A_4}^2 Gr\beta h^6}{12} + \frac{A_4 Gr^2\beta^2 h^8}{96}\right)$$

$$B_4 = \left(\frac{3}{3h^2-h^3}\right)\left(\left(\frac{m-1}{2}\right)\left(\frac{{A_4}^3 h^5}{5} - {A_4}^3 h^4 + \frac{Gr^3\beta^3 h^{11}}{2376} - \frac{Gr^3\beta^3 h^{10}}{216} + \frac{{A_4}^2 Gr\beta h^7}{14} - \frac{{A_4}^2 Gr\beta h^6}{2} + \frac{A_4 Gr^2\beta^2 h^9}{108} - \frac{A_4 Gr^2\beta^2 h^8}{12}\right) - \left(\frac{\boldsymbol{Q_1}+2h}{2}\right)\right)$$

4. Results and Discussion

Figs. 4-9 illustrate the behavior of the axial velocity profile of the flowing bile in the presence of stone characterized by Carreau's fluid model at a particular instant of time for different values of Grashof number Gr, Knudsen number Kn, source-sink parameter β, power index m and amplitude ratio ϕ.

In Fig. 4 two cases are considered, (i) $Gr > 0$, (when the duct wall is in cooling condition) as Gr increases axial velocity decreases. Whereas in case (ii) when $Gr < 0$ (when the duct wall is in heating condition), reverse style of axial velocity is noticed. This trend is observed at x= 0.5 at certain points of the duct. As bile contacts with stone, the bile velocity is more in case of cooling condition and noticed that the velocity of bile is decreased in stenosed region $x\epsilon(0.3,0.65)$ and also observed maximum decay at $x = 0.5$. In a comparison of heating and cooling conditions, the axial velocity is more in the case of the cooling condition.

Fig. 5 describes the impact of wall slip parameter Kn on the axial velocity with axial distance, this shows that the axial velocity decreases as increases slip parameter and also observed that the velocity decreases more in the region $x\epsilon(0.3,0.65)$ this region represents the obstacle region or calculus region, it produces resistance to flow the bile in a duct.

Fig. 6 shows the different values of power index m, it is observed that $m > 1$velocity quickly decreases, which means for highly viscous bile velocity is decreases more as compared with low viscous bile due to obstacle. It is also observed that the value of the axial velocity is greater than those in case of shear-thinning behavior $m < 1$ and also for shear-thinning $m > 1$ and observed that the velocity curve in the axial distance shows valley in $x\epsilon(0.3, 0.65)$ region this region represents calculus part of the duct.

From Fig. 7 it is noticed that axial velocity decreases as the amplitude ratio increases. A high amplitude ratio leads to a decreased cross-section during bolus propagation, so the axial velocity decreases at high amplitude wave and observed that minimum velocity in stenosed region $x\epsilon(0.3,0.65)$.

Fig. 8 shows the variation of axial velocity with axial distance for different source/sink parameter values and observed that the axial velocity decreases on increasing source/sink parameter. It produces heat due to the flow of bile in a duct; it leads to changes in temperature over the wall duct effect the axial velocity.

Fig. 9 describes the impact of the height of stenosis on the axial velocity with axial distance; curves clearly show the axial velocity decreases as the height of stenoses increases. It also observed that maximum decay in velocities at a maximum height of the stenosis produces maximum resistance in the path of bile flow—the obstacle region $x\epsilon(0.3,0.65)$.

Figs. 10-14 illustrate the behavior of the pressure gradient distribution of the flowing bile in the presence of stone characterized by Carreau's fluid model at a particular instant of time for different value of Grashof number Gr, Knudsen number Kn, source/sink parameter β, power index m and amplitude ratio ϕ.

Fig. 10 reports two cases of Gershoff Gr, in case (i) $Gr > 0$ (cooling condition of duct wall) on increasing Gr, pressure gradient decreases, it means changing pressure with axial distance is reduced in cooling/freezing condition and clearly observed the peak of pressure gradient in the curve corresponding to the calculus, this implies that the pressure maximum at $x = 0.5$ is the maximum height of the stone at $x = 0.5$. The stenosed region represents $x\epsilon(0.3,0.65)$. In case(ii) when $Gr < 0$ (heating condition of duct wall) converse trend is observed, it means pressure gradient increases as we increase the temperature of the duct wall. It helps to increase the velocity of the fluid, so more pressure is required in the blockage region to maintain the same flux.

Fig. 11 shows the variation of pressure distribution with the axial distance it is seen pressure increases on increasing Kn. It means more pressure is required to maintain the same flux as we increase the slip parameter; it is clearly observed that maximum pressure is in the stenosed region $x\epsilon(0.3, 0.65)$.

Fig.12 depicts pressure gradient has two phases, i.e., $m > 1\ and\ m < 1$, this shows on increasing fluid behavior index, the pressure gradient also increases. When the fluid behavior index increases, it means the viscous force of the fluid increase due to the high viscous force the bile is thick, so more pressure is required to maintain the same flux. It clearly shows that the maximum pressure is required in the blockage region $x\epsilon(0.3,0.65)$.

Fig. 13 displays the pressure distribution with axial distance for different values of source/sink parameter. We observed that the pressure gradient decreases on increasing source/sink parameter, it means heat increases on the duct wall, and the produced heat is due to the flow of bile in the duct.

Fig. 14 shows the variation of pressure distribution with axial distance for different values of amplitude ratio, pressure gradient increases on increasing the amplitude ratio. It means more pressure is required to maintain the same flux throughout the duct at a high amplitude ratio. A high amplitude ratio leads to a decrease in the cross-section during bolus propagation. It can be seen maximum pressure occurs at $x = 0.5$ and less pressure is required in wider part $x\epsilon(0,0.3)U(0.65,1)$ of the duct.

Fig. 15 displays the variation of pressure distribution with axial distance for different stenosed heights. The pressure gradient increases on increasing the height of the stenosis and noticed that obstacle size increases in the duct, so more pressure is required to maintain the same flux in thein obstacle region $x\epsilon(0.3,0.65)$. At the maximum height of the stenosis, maximum pressure is required to maintain the same flux through the duct.

Figs. 16-19 display the results of calculated pressure rise in terms of average flux with different emerging parameters. All plotted graphs represent the linear relationship between pressure rise and average flux. The pumping phenomenon can be classified into three regions, where the change in pressure rise is carried out. The region $\Delta P > 0$ is known as the pumping region and is also called a positive pumping region for $\Theta > 0$. If $\Delta P < 0$ is known as co-pumping region and $\Delta P = 0$ is called a pumping-free region.

Fig. 16 depicts the variation of pressure rise with average flow rate for different values of Gershoff number, it is noticed when varying $Gr > 0$ then decrement in pressure

rise for a given flux. It is also observed that the pressure rise is less decreasing for the high value of Gershoff number Gr.

Fig. 17 displays the variation of pressure rise with average flow rate for different values of power index m. We noticed that for a large value of fluid behavior index, the pressure rise decreases for given flux and also observed that the value of fluid behavior index $m > 1$ the pressure rise is more decreasing comparatively.

Fig. 18 shows the variation in pressure rise with average flux for different values of source/sink parameter; it is noticed as we increase the source/sink parameter, the pressure rise decreases linearly. It is also observed that for a higher value of source/sink parameter, the pressure rise is increasing comparatively.

Fig. 19 displays the variation of pressure rise with average flux for different values of Knudsen number and noticed that the pressure rise decreases on increasing the slip parameter.

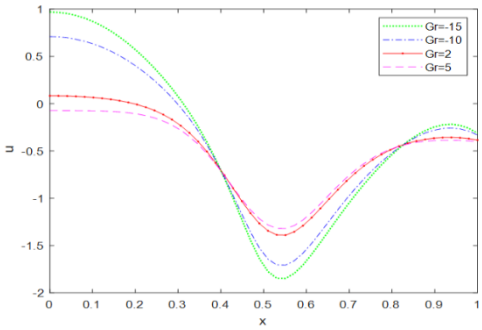

Fig. 4. Axial velocity profile for different Gershoff number (Gr) at $k_n = 0.5, We = 0.1, a = 0.005$ $\beta = 0.5, \delta = 0.1,$ m=0.56, ϕ=0.5, λ=0.5, $x_0 = 0.3$

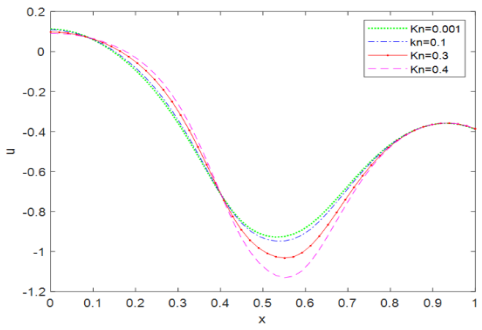

Fig. 5. Axial velocity profile for different Knudsen number (k_n) at Gr $= 5, We = 0.1, a = 0.005,$ $\beta = 0.5, \delta = 0.1,$ m=0.56, ϕ=0.5, λ=0.5, $x_0 = 0.3$

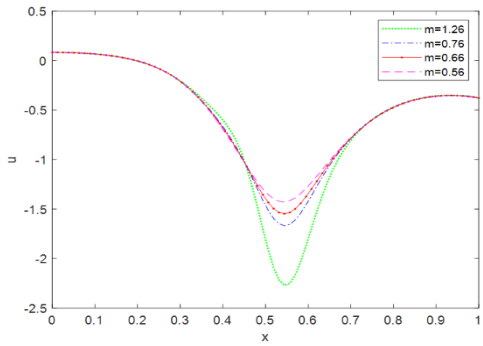

Fig. 6. Axial velocity profile for different fluid behavior index (m) at $Gr = 5,\ k_n = 0.5, We = 0.1, a = 0.005,\ \beta = 0.5, \delta = 0.1,$ ϕ=0.5, λ=0.5, $x_0 = 0.3$

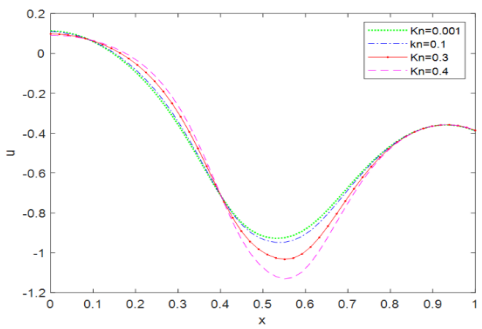

Fig. 7. Axial velocity profile for different amplitude ratio ϕ $Gr = 5, k_n = 0.5, We = 0.1, a = 0.005,$ $\beta = 0.5, \delta = 0.1,$ m=0.56, λ=0.5, $x_0 = 0.3$

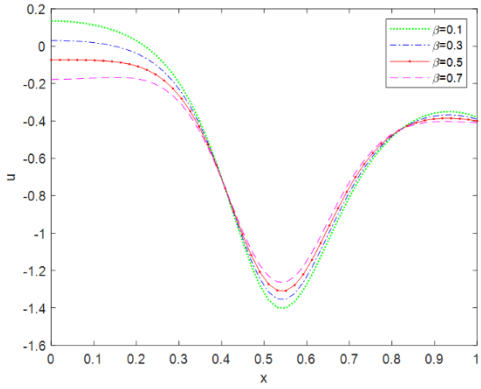

Fig. 8. Axial velocity profile for different source and sink parameter β at $Gr = 5,\ k_n = 0.5, We = 0.1, a = 0.005, \beta = 0.5, \delta = 0.1$ m=0.56, ϕ=0.5, λ=0.5, $x_0 = 0.3$

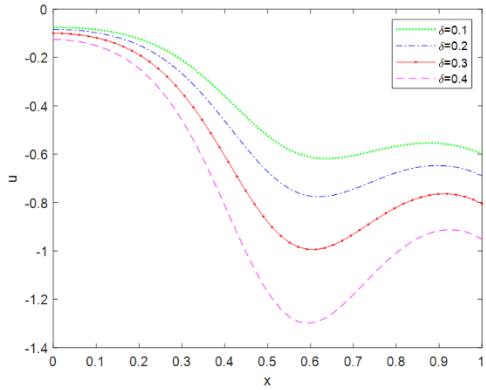

Fig. 9. Axial velocity profile for different height of stenosis index (m) at $Gr = 5,\ k_n = 0.5, We = 0.1, a = 0.005,\ \beta = 0.5, m = 0.56$ ϕ=0.5, λ=0.5, $x_0 = 0.3, x_0 = 0.3$

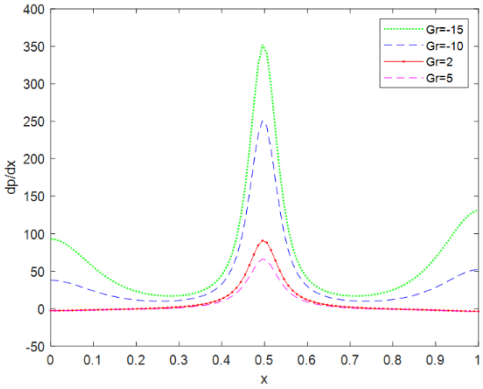

Fig. 10. Pressure gradient profile for different Grash of number (Gr) at $k_n = 0.5, We = 0.1, a = 0.005,\ \beta = 0.5, \delta = 0.1,$ m=0.56, ϕ = 0.5, λ = 0.5, $x_0 = 0.3$.

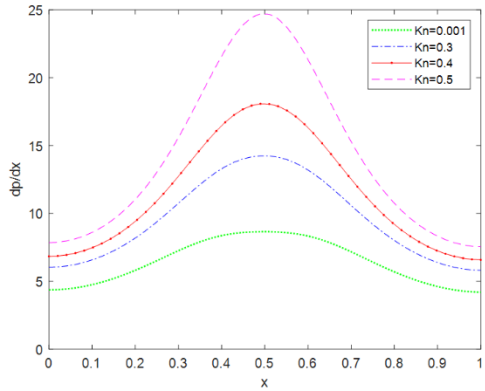

Fig. 11. Pressure gradient profile for different Knudsen number (k_n) at Gr $= 5, We = 0.1, a = 0.005, \beta = 0.5, \delta = 0.1,$ m=0.56, ϕ = 0.5, λ = 0.5, $x_0 = 0.3$.

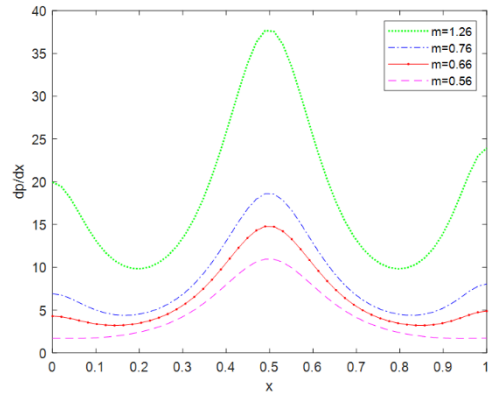

Fig. 12. Pressure gradient for different power index (m) at , Gr $= 5$, $k_n = 0.5, We = 0.1, a = 0.005$, $\beta = 0.5, \delta = 0.1$, $\phi = 0.5$, $\lambda = 0.5$, $x_0 = 0.3$.

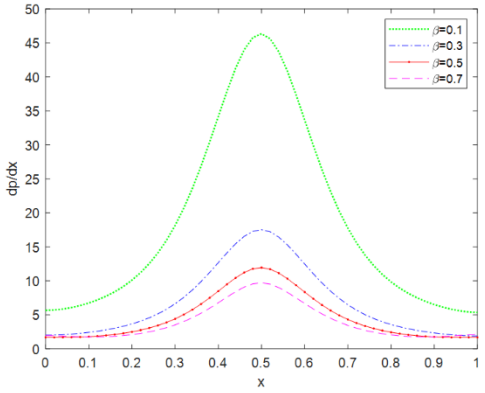

Fig. 13. Axial velocity profile for different source and sink parameter(β) at Gr $= 5$, $k_n = 0.5, We = 0.1, a = 0.005, \delta = 0.1$, m = 0.56, $\phi = 0.5$, $\lambda = 0.5$, $x_0 = 0.3$.

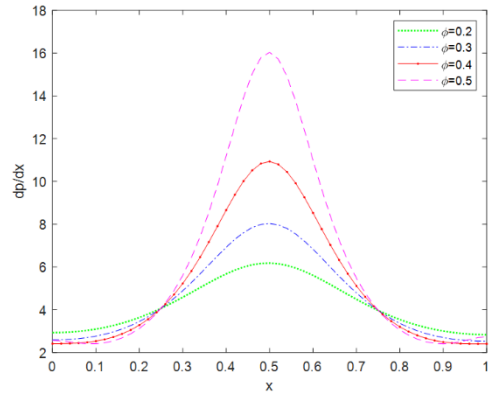

Fig. 14. Pressure gradient profile for different amplitude ratio ϕ at $Gr = 5, k_n = 0.5, We = 0.1, a = 0.005, \beta = 0.5, \delta = 0.1$, m = 0.56 $\lambda = 0.5$, $x_0 = 0.3$.

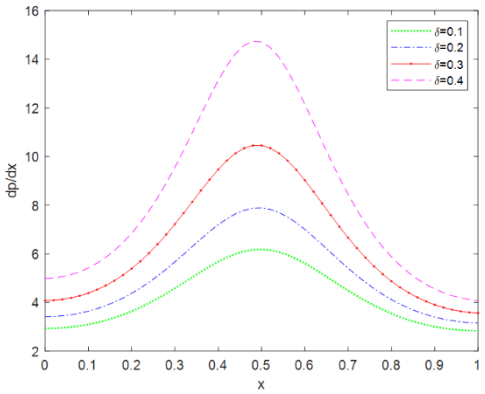

Fig. 15. Pressure gradient for height of stenosis (δ) at, Gr $= 5, k_n = 0.5, We = 0.1, a = 0.005$, $\beta = 0.5$, m = 0.56, $\phi = 0.5, \lambda = 0.5$, $x_0 = 0.3$

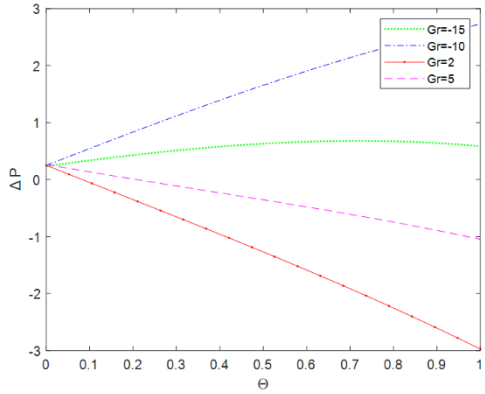

Fig. 16. Pressure rise versus flow rate for different value of Grashof number(Gr) at $k_n = 0.5, We = 0.1, a = 0.005, \beta = 0.5, , \delta = 0.1$ m = 0.56, ϕ= 0.5, λ = 0.5, $x_0 = 0.3$.

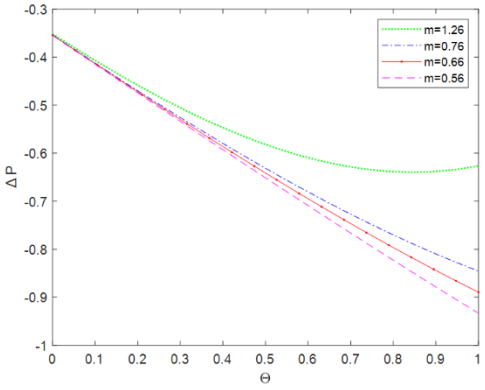

Fig. 17. Pressure rise versus flow rate for different power index (m) at $Gr = 5, k_n = 0.5, We = 0.1, a = 0.005, \beta = 0.5, \delta = 0.1$ ϕ = 0.5, λ = 0.5, $x_0 = 0.3$.

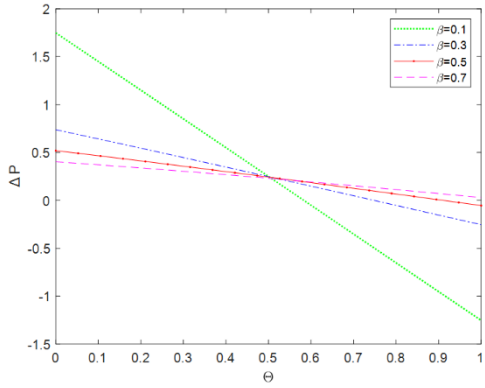

Fig. 18. Pressure rise versus flow rate for different source and sink parameter (β) at Gr = 5, $k_n = 0.5, We = 0.1$, $a = 0.005, \delta = 0.1$, m = 0.56, ϕ = 0.5, λ = 0.5, $x_0 = 0.3$.

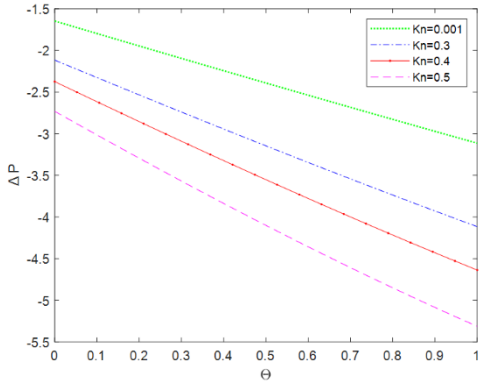

Fig. 19. Pressure rise versus flow rate for different Knudsen number (k_n) at Gr = 5, $We = 0.1, a = 0.005, \beta = 0.5, \delta = 0.1$ m = 0.56, ϕ = 0.5, λ = 0.5, $x_0 = 0.3$.

5. Conclusion

This mathematical model is solved analytically for peristaltic transport of lithogenic bile through a calculus duct under the effect of heat transfer with wall slip conditions and studied the effect of emerging parameters i.e., source/sink parameter, Grashof number, Knudsen number, amplitude ratio and fluid behavior index on axial velocity, pressure gradient and pressure rise. Here we considered two dimensional equations and these equations are simplified using low Reynolds number and long wavelength approximation.

Adopting the perturbation technique, analytical expressions for axial velocity, pressure rise, and pressure gradient are drawn with MATLAB R2018b software. This paper has physical significance because it deals with a diseased biliary tree (small gallstones blocks the ducts) Results can be summarized as the following points.

- In case of Grashof number, two different patterns of velocity are noticed, velocity increases as varying heat source/sink parameter and also observed that maximum decay in velocity at maximum blockage part.
- Axial velocity decreases in stenosed region $x\epsilon(0.3,0.65)$ on increasing slip parameter, fluid behavior index and the height of stenosis.
- Pressure gradient also shows two different patterns for Grashof number, more pressure is required to maintain flux in cooling condition.
- When heat source/sink parameter, Weissenberg number and amplitude ratio increases, pressure gradient also increases and it is observed that the maximum pressure occurs in stenosed region $x\epsilon(0.3,0.65)$.
- It is possible boost pressure rise for all effecting parameter of the model.

The present study is directly related to the modelling of the bile flow for a non-Newtonian fluid in the duct with calculus. The patient-specific mathematical model created, allows us to estimate the dynamics of the postoperative period, and this information helps to predict complications during surgery on the basis of pressure distribution data of bile. It also helps to find the position and size of stone in the ducts and notice the effect of temperature on the bile flow; it concludes some important results that velocity and the pressure vary with cooling and heating condition.

Reference

1. A. I. Edemskiy and D. A. Edemskiy, Russian Surgery Bul. **7**, 35 (2002).
2. S. Agarwal and A. K. Shina, Int. J. Appl. Math. Mech. **8**, 92 (2012).
3. S. Maiti and J. C. Misra, Int. J. Eng. Sci. **49**, 950 (2011). https://doi.org/10.1016/j.ijengsci.2011.05.006
4. A. G. Kuchumov, Y. I. Nyashin, and V. A. Samartsev, 7th WACBE World Congr. Bioeng. 52, 158 (2013). https://doi.org/10.1007/978-3-319-19452-3_42
5. S. Srinivas and R. Muthuraj, Int. J. Appl. Mech. **2**, 437 (2010). https://doi.org/10.1142/S1758825110000573
6. A. A. Khan, R. Ellahi, and M. Usman, J. Porous Media **16**, 59 (2013). https://doi.org/10.1615/JPorMedia.v16.i1.60
7. A. G. Kuchumov, Russian J. Biomechanics (2016). https://doi.org/10.15593/RJBiomech/2016.2.01
8. N. Maheshbabu and S. Sreenadh, J. Math. Comput. Sci. **10**, 1083 (2020). https://doi.org/10.28919/jmcs/4539
9. W. Mahmood, M. Sajid, M. N. Sadiq, and N. Ali, Pramana **95**, ID 7 (2021). https://doi.org/10.1007/s12043-020-02055-z
10. J. S. Goud, P. Srilatha, L. Indira, B. Raju, and A. Praveen, J. Nat. Remedies **21**, 18 (2020).
11. S. K. Pandey and D. Tripathi, Int. J. Biomathematics **3**, 473 (2010). https://doi.org/10.1142/S1793524510001094
12. D. Tripathi and J. Mazumdar, J. Bionic Eng. **14**, 643 (2015). https://doi.org/10.1016/S1672-6529(14)60154-2

13. S. Kumari, T. K. Rawat, and S. P. Singh, J. Sci. Res. **13**, 821 (2021). https://doi.org/10.3329/jsr.v.2.029 13i3.52487
14. R. C. Ooi, X. Y. Luo, S. B. Chin, A. G. Johnson, and N. C. Bird, J. Biomech. **37**, 1913 (2004). https://doi.org/10.1016/j.jbiomech.2004.02.029 15
15. A. G. Kuchumov, Y. I. Nyashin, V. A. Samarcev, and V. A. Gavrilov, Acta Bioeng. Biomech. **15**, 9 (2013). https://doi.org/10.5277/abb130402
16. A. G. Kuchumov, V. Gilev, V. Popov, V. Samartev, and V. Gavrilov, Korea Aust. Rheol. J. **26** 81 (2014). https://doi.org/10.1007/s13367-014-0009-1
17. N. T. M. El-Dabe, G. Moatimid, M. Gaber, and D. R. Mostapha, Appl. Math. Inf. **10**, 673 (2016).